COMSOL Simulations for Scanning Microwave Microscopy

T. Le Quang, D. Vasyukov, J. Hoffman, A. Buchter, M. Zeier
Federal Institute of Metrology (METAS), Bern, Lindenweg 50, 3003 Bern-Wabern, Switzerland

Introduction

Scanning microwave microscopy (SMM) belongs to scanning probe techniques, which allow studies of various material properties on nanometer scale. Apart from the topography of the sample, SMM can measure its electrical properties. The characterization is performed by measuring the reflection coefficient S_{11} of high-frequency electromagnetic signals from the sample surface. Such experiments have been demonstrated in a variety of materials, e.g. semiconductor structures [1], 2D materials [2] and complex oxides [3]. The use of the SMM techniques in industry, however, is hindered by the calibration difficulties.

In order to solve this problem, the METAS team has modified the "short-open-load" (SOL) calibration approach, which is well-known in microwave engineering. As demonstrated in [4], the SMM measurements performed on three samples with known capacitance (standards), one can calibrate the SMM setup by acquiring a set of three error coefficients. Following this calibration step, one can estimate the capacitance of an unknown device under test (DUT) from its measured S_{11}. Recent SMM studies performed in METAS for vertical GaAs heterostructures allowed successful measurement of their doping density [5].

To support our future experimental activities performed on devices with lateral structures, we simulate these experiments using COMSOL multiphysics software. Resulting electromagnetic models will provide a deeper understanding of our measurements. The details of our SMM setup and of our models, followed by simulation results for various types of lateral structures, are explained below.

Theory / Experimental Set-up

A sketch shown in Fig. 1a illustrates the main part of our SMM setup, where the tip is in contact with a sample. The tip is several millimeters long and has the other end connected to a vector network analyzer (VNA), via coaxial lines and an impedance matching network. The total length of the connection is less than 1 m. The SMM tip is made from a metallic (Platinum/Iridium) wire with a diameter of 0.5 mm by electrochemical etching to obtain a sharp apex with a diameter of few tens of nanometers. In our

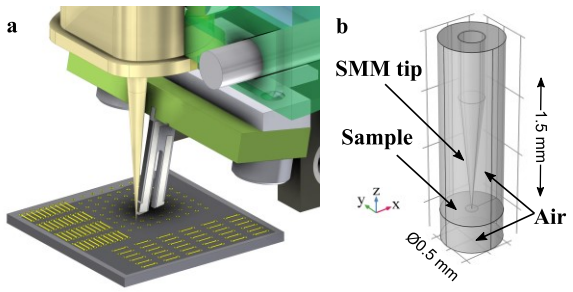

Figure 1 | a, Sketch of a scanning microwave microscope head showing the tip in contact with a sample. **b**, Simplified model used in our simulations.

setup, the VNA provides signals between 1 GHz and 50 GHz. Samples, which were fabricated and will used in real experiments, have a square shape with an area of ~5x5 mm^2 containing a large number of small patterns, by depositing and removing selectively parts of a 100 nm thick metallic bilayer (95 nm thick Au and 5 nm thick Ti). This film is supported by a 500 nm thick SiN membrane, as shown in Fig. 2a. On each sample we were able to prepare multiple patterns, which can be divided into three types:

- Type I, which is presented in Fig. 2b has an exposed SiN region (gray area) completely separating the two Au regions (blue): the landing pad and the ground plane.
- Type II (Fig. 2c) has a small and straight Au bridge connecting the landing pad and the ground. The width of this bridge is 200 nm.
- Type III (Fig. 2d) has a curvy/spiral-like bridge. The width of this bridge is 200 nm.

While devices of Type I are expected to behave as a capacitor, the others should work as electrical circuits with a resistor due to having their conducting Au bridge. Samples of Type III were designed with many rings to acquire an inductance via the interaction between its rings.

Concerning the calibration technique, as described in the Ref. [4], by viewing the SMM and the VNA as a linear microwave network, authors find that the SOL algorithm used in the VNA calibration can be also applied to SMM measurements. In this approach, the impedance, Z_{tip}, measured by the tip in reality can be related to the S_{11m} obtained from SMM measurements or their COMSOL simulations using the following formulae:

Excerpt from the Proceedings of the 2018 COMSOL Conference in Lausanne

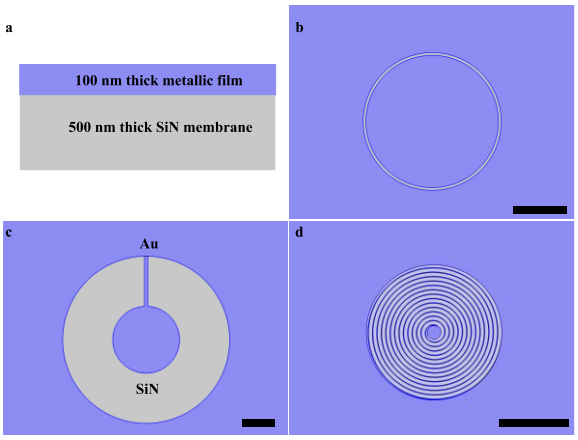

Figure 2 | **a,** Sketch of samples which are used in our simulations. In reality, they were fabricated by depositing a 100 nm thick Au/Ti films on a 500 nm thick SiN membrane. By removing selectively parts of the deposited materials, we created various structures: without any conducting path (type I), with a straight short metallic bridge (type II), or with a long bridge with a spiral form (type III). Examples of these patterns are presented in **b, c,** and **d**, accordingly. In these drawings, the blue regions represent the metallic surface (Au/Ti bilayer), and the gray ones – SiN membrane, where the film was removed. Scale bars in panels **b**, **c** and **d** are 5 µm, 2 µm and 20 µm accordingly.

$$S_{11} = \frac{Z_{tip} - Z_{ref}}{Z_{tip} + Z_{ref}} \qquad (1)$$

$$S_{11m} = e_{00} + \frac{S_{11} e_{01}}{1 - S_{11} e_{11}} \qquad (2)$$

Here, Z_{ref} has an arbitrary non-zero value. For the following calculations presented in the "**Results**" section, we chose Z_{ref}=5-0.1*i*. S_{11} is the reflection parameter in the ideal situation, where signals travel back and forth between the VNA and the sample without any unwanted reflections at connectors between the tip and the VNA. To take into account these losses, three error coefficients, e_{00}, e_{01} and e_{11}, are introduced, which can be extracted from S_{11m} obtained for three devices, which play the role of standards. Their Z_{tip} values are obtained from COMSOL simulations as a ratio of the flowing current in the tip, *I,* and the voltage drop on the sample, *V*, using the following formulae:

$$I = \int \vec{H}.d\vec{l} \qquad (3)$$

$$V = -\int \vec{E}.d\vec{s} \qquad (4)$$

While the line integral in Eq. 3 is performed along a closed circle in a plane staying 3 µm above the sample surface, the one written in Eq. 4 is done along a straight line on the sample surface along the *x*-axis connecting the landing pad and the outer boundary.

Table 1. List of samples (standards and DUTs) used in this paper and their Z_{tip} calculated using Eq. 3 and 4, inouts of which were obtained from simulations performed at 1 GHz in the presence of a sharp tip (0.2 µm apex diameter).

Type of circuits	Standard 1 (Ohm)	Standard 2 (Ohm)	Standard 3 (Ohm)	DUT (Ohm)
Type I	0-84342i	0-47311i	0-10963i	2.384-15574i
Type II	0.707-0.008i	10.280-0.019i	22.508-0.027i	16.394-0.023i
Type III	25.159+0.090i	48.784+0.206i	992.97+7.190i	249.61+1.142i

Once these error coefficients are known, the SMM set up is calibrated and we are able to determine the impedance of the DUT, which shares the same design with three standards, from its S_{11m} as below:

$$S_{11} = \frac{S_{11m} - e_{00}}{e_{01} + e_{11}(S_{11m} - e_{00})} \qquad (5)$$

$$Z_{extracted} = Z_{ref} \frac{1 + S_{11}}{1 - S_{11}} \qquad (6)$$

This impedance will be then compared with the Z_{tip} got from simulations for the device. A small or even zero difference between these two values proves the applicability of the SOL technique for the SMM measurement performed on that specific type of device in the used condition (frequency and tip). Then, the whole process needs to be repeated for simulations using different DUTs and different tips for frequencies varying from 1 GHz to 50 GHz (the working range of our VNA). The two later would allow us to check the frequency independence and the tip independence of the SOL method.

Because the verification of the SOL technique requires the presence of three standards and of at least one DUT, for each type of lateral structures we use four devices with different impedance. Then, the impedance of these four devices is varied via the use of different sets of parameters, like the gap between the landing pad and the ground plane, or the number of rings (for the spiral bridge), while keeping the geometry unchanged. The same technique will be also applied for real devices. The impedance Z_{tip} for all samples are listed in Table 1.

COMSOL models and simulations

To simulate SMM experiments, we employed mainly the Electromagnetic Wave interface in the AC/DC module. Because we are interested in checking the frequency dependence of the calibration algorithm, all simulations were performed using the time domain interface. "Finer" meshing was used for the most of the

simulations; otherwise the meshing specifics are indicated in the text.

As written above, in a real-world SMM the tip (apex diameter ~10^1 nm) is on the one end connected to the VNA via coaxial lines and an impedance matching network and its sharp end is in contact with a 100 nm thick Au film with an area of ~5x5 mm^2. This thin film in turn contains many nanometer-sized features. While simulations for models with all these details would provide a full understanding of our system, such a calculation would demand a huge computational power and take an enormous amount of machine time. Therefore, in this study, it is critical to construct a simplified model, so that the simulations can be done efficiently.

First, as shown in Fig. 1b we removed a large part of our setup and only focused on a few millimeters long part of the tip and the sample. Consequently, the electromagnetic interaction of removed parts of the microscope with the sample is ignored. The SMM tip is also simplified in our model as a combination of a cylinder and a truncated cone. The cylindrical part has a diameter of 0.2 mm and is 0.5 mm tall. The conical part has a height of 1 mm and a diameter of 0.2 mm at the connecting plane between the two parts. Then, to get different tips, we varied the diameter of the tip apex, where the tip is in contact with the sample. In this article, we will present the data obtained from simulations, which have tips with an apex diameter of 0.2 µm (a new sharp tip) and 2 µm (an old blunt tip).

Second, our samples are also simplified significantly. While real samples have millimeter sizes and consist of many patterns, which are studied with a mobile tip, those used in our simulations have a circular shape with a diameter of 0.5 mm and contain only one pattern in the center of the sample, where the tip lands on. Then, instead of scanning the tip around, we kept it immobile and replaced the studied pattern one after another. Therefore, interactions between tips and other patterns in real samples are ignored in our simulations. In order to verify how these simplifications affect our findings, we need to work with models, where the size of the tip and of the sample differ from those discussed here, however, the influence of these parameters does not affect much our main conclusions.

Apart from the two discussed simplifications, the application of the transition boundary condition (TBC) with the electrical properties of pure gold to simulate the 100 nm thick deposited Au/Ti films also helps us to reduce further the computational effort. Otherwise, other parts, like thick air layers, the SMM tip and the SiN membrane are fully meshed. The outer boundaries of the models are treated as perfectly conducting materials and the coaxial microwave signal is sent and collected at the free end of the SMM tip.

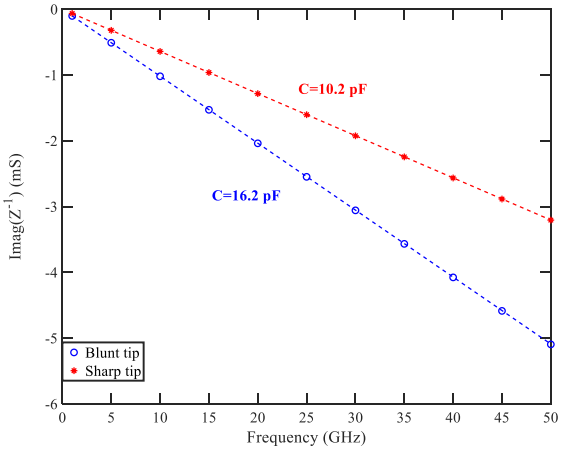

Figure 3 | Tip and frequency dependence of the imaginary part of admittance $Imag(Z_{tip}^{-1})$ for the DUT of the Type I (Fig. 2b). Blue circles and red asterisks were obtained from simulations with the blunt and the sharp tips correspondingly. Dashed lines illustrate the linear behavior of the two sets of data.

Simulation Results

1. Frequency and tip dependence of Z_{tip}

Before the verification of the SOL technique, it is important to verify whether our designs can provide different types of electrical circuits as designed. From designs presented in Fig. 2b, c, and d, we expect to obtain electrical circuits with a capacitor (Type I); with a resistor (Type II); with a resistor and an inductor connecting in series (Type III). While this goal seems to be achieved as evidenced by values listed in Table 1, the frequency dependence of Z_{tip} can provide further confirmation.

We start with the simulations for the pattern Type I (without any conducting connections). Fig. 3 plots the imaginary part of the admittance or $Imag(Z_{tip}^{-1})$ of the DUT as a function of frequency. Blue circles and red asterisks represent data acquired from COMSOL simulations with the blunt and sharp tips accordingly. As shown, $Imag(Z_{tip}^{-1})$ always has a minus sign and its amplitude rises linearly with frequency. These findings point out the capacitive behavior of the DUT, as expected from its design, two separated Au regions of which act as two electrodes of a capacitor.

Furthermore, despite of being obtained from one device, blue circles and red asterisks do not overlap with each other and the difference grows with frequencies. This indicates that the admittance and the capacitance of the DUT depend on the tip, which indeed interacts with the sample. Knowing that the

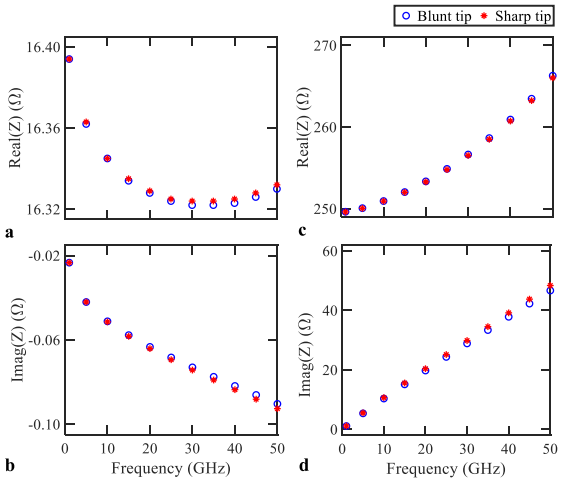

Figure 4 | Tip and frequency dependence of the real and imaginary impedances, *Real(Z_{tip})* and *Imag(Z_{tip})*, obtained for DUT having metallic bridges of various forms: **a** and **b** for the straight bridges and **c** and **d** for the spiral-like bridges. Blue circles and red asterisks were obtained from simulations using a blunt and a sharp tip correspondingly.

obtained admittance depend linearly on frequency, we are able to determine the capacitance of the device from the equation: $C = Imag(Ztip^{-1})/(2\pi f)$, here f is the frequency. Then, values of 16.2 pF and 10.2 pF were obtained for simulations of SMM experiments with the blunt and sharp tips accordingly . Thus, simulations for the Type I sample suggest a strong tip impact and let's check whether similar effect also exists for samples of the Type II and Type III, where a conducting path exists. Figure 4 presents the frequency dependence of *Real(Z_{tip})* and *Imag(Z_{tip})* for DUTs having metallic bridges (Type II and Type III). While data plotted in Figs. 4a, 4c, and 4d has a plus sign as expected for a resistance of such metallic bridges, those shown in Fig. 4b are unexpected and can be understood only with the consideration of the capacitive tip-sample interaction. Such an interaction should also exist in simulations performed for the third DUT sample, but its weak effect or its absence may have appeared from the large inductance, which in turn originated from the spiral geometry of the fabricated bridge. While the tip and samples with Au bridges interact with each other, the tip impact is found weaker here than in previous case of a capacitor. This is evidenced by the good overlapping between blue circles and red asterisks as can be seen in Fig. 4.

In addition to having positive values, the resistance of the long bridge exhibits a monotonic increase (see Fig. 4c), another indicator of such a metallic connection, where a skin effect at high frequencies becomes significant. The absence of a similar curve in Fig. 4a can be explained by considering the resistance of the non-patterned part of

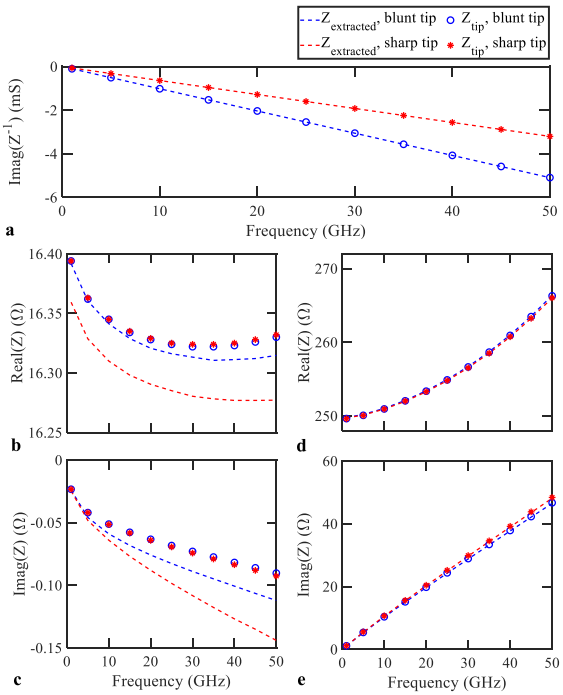

Figure 5 | Comparison of $Z_{extracted}$ (dashed lines and dashed curves) obtained from the calibration technique and Z_{tip} (symbols) for DUT of the **a,** Type I, **b,c,** Type II, and **d,e,** Type III. Blue (red) symbols and curves/lines obtained from simulations using a blunt (sharp) tip. Here, the calibration was done for each DUT using the set of standards of the same type as listed in Table 1.

the gold film, which contributes less in the case with a long and more resistive bridge (Type III). Indeed, by removing the resistance of the non-patterned part, we are able to gain the monotonic increase for the resistance of the Type II sample.

2. Verification of the SOL technique

The analysis above ensures us that the three DUT devices can be treated as three different types of electrical circuits consisting of: only a capacitor (Type I); only a resistor (type II); a resistor and an inductor connected in series (type III). Similar curves (not shown here) are also acquired for standards listed in the Table 1, so that for each type we have three standards and one DUT with the same type of electrical circuit. Our next step is to check whether the SOL technique can provide $Z_{extracted}$ being equal or close to values of Z_{tip} obtained at different frequencies and with different tips.

Figure 5 plots Z_{tip} (symbols) and $Z_{extracted}$ (dashed lines and curves) obtained for the three DUT samples at different frequencies with the two tips. Here, red and blue curves/lines represent $Z_{extracted}$ predicted using the SOL approach for the sharp and blunt tips accordingly. One can easily notice good overlaps between red asterisks (blue circles) and red (blue)

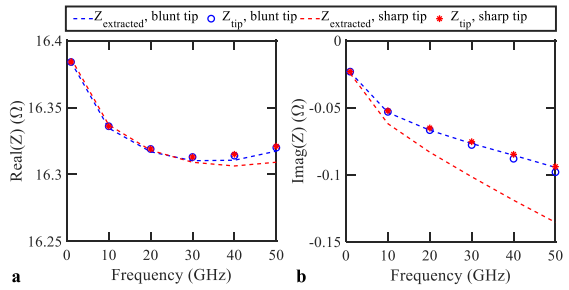

Figure 6 | $Z_{extracted}$ (red and blue dashed curves) and Z_{tip} (blue circles and red asterisks) obtained for DUT of the Type II using an "Extra Fine" meshing.

curves/lines indicating that the SOL approach indeed predicts well the Z_{tip} measured by our SMM tip. Because the same conclusion can be drawn from comparison of data obtained at various frequencies between 1-50 GHz, our simulations predicts that the SOL should work for SMM measurements performed at least in this frequency range.

Furthermore, a difference between Z_{tip} (symbols) and $Z_{extracted}$ up to tens and hundreds of milli-Ohms can be noticed at high frequencies in Fig. 5c and d, accordingly. This difference can result from the two simplifications used in our COMSOL models as well as from the SOL approach. For example, Fig. 6 plots Z_{tip} (symbols) and $Z_{extracted}$ obtained for the DUT of type II like in Fig. 5b and c, but here instead of using "Finer" meshing a more detailed "Extra fine" one is employed. As a result, the difference between Z_{tip} (symbols) and $Z_{extracted}$ is reduced for both real and imaginary parts and in simulations with both sharp and blunt tips.

Conclusion

In conclusion, COMSOL models built for SMM measurements on samples with different lateral structures are presented. Impedances of these types of devices obtained from our COMSOL simulations indicate that they behave as different types of electrical circuits as expected. The comparison between impedance values provided by the short-open-load (SOL) calibration approach and those obtained from COMSOL simulations for all DUTs samples confirms that this technique can be applied to SMM experiments performed for these lateral structures. Moreover, this technique should also work independently from the used SMM tip and at different frequencies between 1-50 GHz. The experimental verification of the SOL approach for real devices will be performed in future.

References

1. M. Kasper *et al.*, Metal-oxide-semiconductor capacitors and Schottky diodes studied with scanning microwave microscopy at 18GHz, *J. Appl. Phys.*, **116**, 184301, 2014

2. Di Wu *et al.*, Uncovering edge states and electrical inhomogeneity in MoS_2 field```-effect transistors, *PNAS*, **113**, 8583, 2016

3. E. Y. Ma *et al.*, Charge-order domain walls with enhanced conductivity in a layered manganite, *Nat. Commun.*, **6**, 7595, 2015.

4. J. Hoffmann *et al.*, A calibration algorithm for near field scanning microwave microscopes, *12th IEEE Conference on Nanotechnology (IEEE-NANO),* 2012.

5. A. Buchter *et al.*, Scanning microwave microscopy applied to semiconducting GaAs structures, *Rev. Sci. Instrum*., **89**, 023704. 2018

Acknowledgements

This research is a part of ADVENT project, which is funded by the European Metrology Programme for Innovation and Research (EMPIR). The goal of this project is to develop nanometrology adapted to characterization of advanced materials for future electronic devices.